Quantifying right ventricular motion and deformation using 3D cine DENSE MRI

D. A. Auger[1], X. zhong[2], E. Meintjes[1], F. Epstein[3], and B. Spottiswoode[1,4]

[1]MRC/UCT Medical Imaging Research Unit, University of Cape Town, Cape Town, Western Cape, South Africa, [2]MR R&D Collaborations, Siemens Medical Solutions, Atlanta, GA, United States, [3]3Departments of Radiology and Biomedical Engineering, University of Virginia, Charlottesville VA, United States, [4]Radiology, University of Stellenbosch, Cape Town, South Africa.

Introduction: The right ventricle is notoriously difficult to image because of its thin wall, asymmetric geometry and unruly motion. Displacement encoding with stimulated echoes (DENSE) is a quantitative MRI technique for measuring myocardial displacement and strain at a high spatial resolution [1,2]. A free-breathing navigator gated spiral 3D cine DENSE sequence has recently been developed [3], thus providing an MRI technique which is well suited to quantifying the complex behavior of the RV. The purpose of this study is to quantify RV motion and surface strain in normal volunteers using 3D cine DENSE MRI.

Methods: Whole heart 3D cine DENSE data was acquired from two normal volunteers on a 1.5T Siemens Magnetom Avanto MRI scanner. The entire heart was imaged in short axis slices at a $2.8 \times 2.8 \times 5$ mm^3 spatial resolution and 32 ms temporal resolution. The displacement was measured in three orthogonal directions. Other imaging parameters include: flip angle = 20°, TR = 16 ms, TE = 1.3 ms, number of spatial interleaves = 6, partitions = 22 and cardiac phases = 22. The endocardial and epicardial contours were manually delineated in order to demarcate myocardium from surrounding anatomical structures. A 3D modified spatiotemporal phase unwrapping algorithm was then used to remove phase aliasing [4]. Cine DENSE allows myocardial motion to be tracked using interpolation at any spatial resolution, and strain can be calculated from the resulting frame-to-frame motion trajectories [4]. Left ventricular (LV) and right ventricular (RV) midline contours were calculated from the epicardial and endocardial contours, and tissue tracking seed points were spaced at pixel-distance intervals along these midlines. The 3D tracking algorithm was implemented as a direct extension of the 2D tracking algorithm presented in [4], and the midline points were tracked through the majority of the cardiac cycle. The motion trajectories were then smoothed by fitting 10th order polynomial functions to each motion trajectory as a function of time for the three Cartesian axis directions. Due to its thin wall, there are typically too few transmural pixels spanning the RV to resolve a full 3D strain tensor. Lagrangian strain was thus calculated from the motion trajectories and oriented along the surface defined by the midline contours. This technique results in reliable tracking and strain quantification but information about radial thickening is lost. For each motion trajectory, the deformation gradient tensor was calculated using two to four nearest neighboring mid line points. Depending on its position in the RV wall, each motion trajectory could have adjacent points to the left and/or right, and on the slices above and/or below. Deformation gradient tensors were then calculated from a minimum of one and a maximum of four sets of co-planar vectors. Unit orthogonal vectors were created perpendicular to the RV surface using cross products for each set of co-planar vectors. Three dimensional Lagrangian strain was then calculated for each deformation gradient configuration and the two principal surface strain components (eigenvectors and eigenvalues) were resolved. These components were then averaged for the various configurations. The strain is calculated using a derivative operation which inherently magnifies noise in the data.

Results: Figure 1 illustrates LV and RV motion at mid and end systole from one of the volunteers at two different views, with the color in the RV depicting first and second principle strains. The results were similar for the second volunteer. The first principle strain (E1) depicts cross-fiber shortening and the values are slightly less than previously reported results from myocardial tagging [5]. The second, or minimum, principle strain (E2) corresponds to the maximum tissue shortening and the values lie within the range reported in [5]. Figure 2 shows an example of the first and second principle eigenvectors at mid systole. The eigenvector directions are reasonably consistent with previous tagging results in diastole [6] and systole [5]. However, given the high spatial resolution achievable here, local eigenvector variations are evident and these are consistent across several RV anatomical regions. High strain is also evident near the RV insertion points.

Conclusion: This work presents 3D RV motion tracking and strain quantification at a previously unattainable spatial resolution. This allows local variations to be identified in RV motion and strain, and paves the way for a more detailed understanding of RV kinematics. Future work will include detailed strain-time analysis in discrete functional regions of the RV, and mapping of mechanical dyssynchrony where the strain propagation can be conveniently portrayed along the midline surfaces.

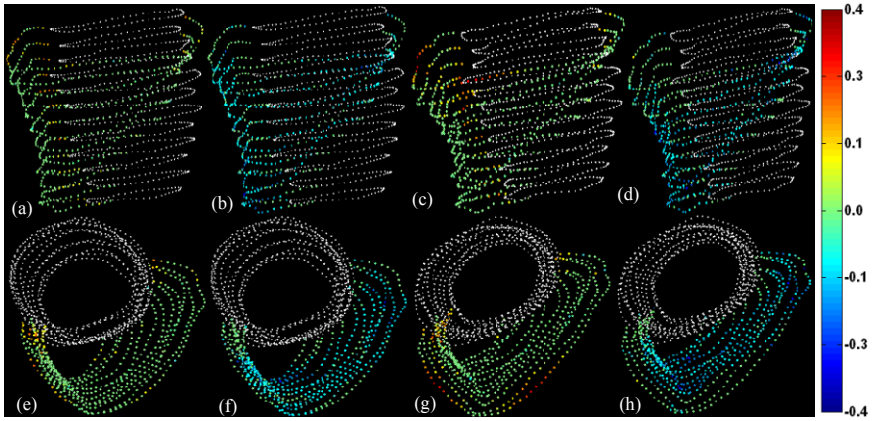

Figure1: 3D RV surface strain images at two points in systole. (a,e) First principle strain at mid-systole, (b,f) second principle strain at mid-systole, (c,g) first principle strain at end-systole, (d,h) second principle strain at end-systole. Dots represent the motion trajectory position while color represents strain

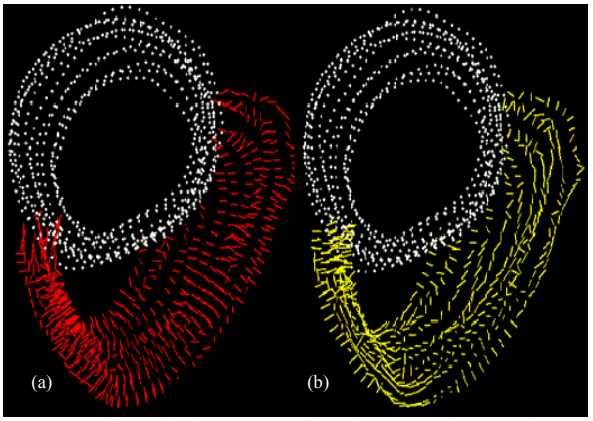

Figure 2: Mid-systolic eigenvector configuration representing E1(red) and E2 (yellow) directions. (a,b) eigenvectors during mid -systole

References: 1. Aletras et al. Journal of Magnetic Resonance 137:247–252 (1999). **2.** Kim et al. Radiology, 230(3):862-871 (2004). **3.** Zhong et al. Proc ISMRM 2009; #17. **4.** Spottiswoode et al. IEEE Transactions on Medical Imaging, 26(1):15-30 (2007) **5.** Haber et al. *AJP - Heart* 289:1826-1833 (2005) **6**. Young et al. AJ P - Heart, 271(6):2677-2688 (1996).